Regulation of Turing patterns in a spatially extended chlorine–iodine–malonic-acid system with a local concentration-dependent diffusivity

Wei-Shen Li,[1] Wen-Yong Hu,[1] Ya-Chun Pang,[1] Tai-Ran Liu,[1] Wei-Rong Zhong,[2] and Yuan-Zhi Shao[1,*]

[1]*School of Physics and Engineering, Sun Yat-sen University, Guangzhou 510275, China*

[2]*Department of Physics and Siyuan Laboratory, College of Science and Engineering, Jinan University, Guangzhou 510632, China*

(Received 10 October 2011; revised manuscript received 12 March 2012; published 28 June 2012)

A chlorine–iodine–malonic-acid Turing system involving a local concentration-dependent diffusivity (LCDD) has fundamental significance for physical, chemical, and biological systems with inhomogeneous medium. We investigated such a system by both numerical computation and mathematical analysis. Our research reveals that a variable local diffusivity has an evident effect on regulating the Turing patterns for different modes. An intrinsic square-root law is given by $\lambda \sim (c_1 + c_2 k)^{1/2}$, which relates the pattern wavelength (λ) with the LCDD coefficient (k). This law indicates that the system pattern has the properties of an equivalent Turing pattern. The current study confirms that, for the Turing system with LCDD, the system pattern form retains the basic characteristics of a traditional Turing pattern in a wide range of LCDD coefficients.

DOI: 10.1103/PhysRevE.85.066132 PACS number(s): 82.40.Ck, 47.54.−r, 64.60.an, 89.75.Da

I. INTRODUCTION

Pattern formation is a ubiquitous phenomenon in the physical, chemical, biological, and ecological fields [1]. The Turing pattern, as a representative type of pattern confirmed by the Lengyel's experiment of chlorine–iodine–malonic acid (CIMA), has been subjected to extensive studies [2,3]. Many factors play important roles in regulating and manipulating pattern form. Studying the influence of such factors on the Turing pattern becomes a major issue in Turing pattern formation.

Depending on the nature of regulation, the mechanism underlying regulation of pattern forms can be generally classified into three categories: an intrinsic mode, an external mode, and a noise mode.

The intrinsic mechanism refers to the development of many biochemical patterns, and functions through adjustment of parameters or models themselves. Maini and co-workers have figured out some patterns with high similarity to some special animal skin patterns by coupling and tuning two Turing systems with different controlling parameters [4–6]; their simulation results have been confirmed by Kondo and Miyazawa in a certain type of fish pattern observed in nature [7,8]. The extrinsic mechanism consists in regulating the pattern of a Turing system driven by an external field. The intensity, time, and directionality of an applied field plays a main role in the transitions between different types of Turing patterns [9–14]. Noise, due to the fluctuation of either internal or external factors, acts as a new dimension for pattern regulation and contributes to some new pattern formation by altering its intensity and formulation [15–18].

Diffusion is also a crucial factor in pattern formation for a reaction-diffusion (RD) system. For the sake of simplification, the diffusion coefficient is usually set as a constant in a conventional RD model [19,20]. This oversimplified approach is not suitable for most RD systems, especially a biological system with heterogeneity.

Research on morphogens in the synthesis-diffusion-degradation (SDD) model demonstrates that the local concentration-dependent dynamic behavior, which will eliminate or buffer against the influence of the genetic or environmental fluctuation, can gain a more precise morphogen gradient formation [21–23]. Beyond the SDD model, it is rational to extend the local concentration-dependent diffusivity (LCDD) approach to a Turing system that is sensitive to local concentration-dependent dynamic behavior as well. The relevant approach is implemented to regulate the Turing pattern through introducing an effective parameter, i.e., LCDD coefficient. As a motivation of our current investigation, the study of the LCDD in a Turing system will be useful to gain insight into the mechanism of intricate pattern formation in a RD system. Meanwhile, our ideas originated from a series of interesting findings by Japanese scientists [24–28]. According to their studies, the diffusivity, acting as a key factor in pattern formation, can lead to preferred directionality of the Turing stripe pattern. By analogy to this theory, introducing a LCDD probably brings in a novel concentration distribution of reactant. In addition, a common phenomenon of the deformation of the medium during the chemical reaction is also related to LCDD [29].

Local concentration-dependent diffusion in a RD system has attracted much attention in a variety of fields [30–32]. Malchow's study indicates that both the symmetry and the amplitude of patterns vary considerably due to the introduction of LCDD [33]. Roussel and Wang applied the first order expression of the diffusion coefficient to the one-dimensional (1D) and two-dimensional (2D) excitable media, and observed a unique pattern form that is different from a traditional Turing pattern [34,35]. The evolutional behavior of a LCDD CIMA Turing RD system is not yet fully studied due to the involvement of complicated reaction terms, the difficulty in linear stability analysis, and little evidence available in experiment. How does the pattern of the Turing system evolve after introducing a LCDD? Is there a specific relationship in the LCDD Turing system that relates the pattern wavelength with the variable diffusion coefficients? In this paper, we will address these two problems.

*Author to whom correspondence should be addressed: stssyz@mail.sysu.edu.cn

The remainder of the paper is organized as follows. In Sec. II, we describe the LCDD Turing model and the method for quantitative image processing used to classify patterns. In Sec. III, we present the results of pattern formation with different spatiotemporal parameters; the relationship concerning the pattern wavelength, system size L, and LCDD coefficient k, and a theoretical analysis for the simulated results is given. The concluding remarks are included in Sec. IV.

II. MODEL AND METHOD

A. Model and modification

In this study, the CIMA activator-inhibitor model (Lengyel-Epstein model) [3,36] was selected as the basic model to investigate the pattern regulation of a Turing system with a LCDD. The dimensionless reaction-diffusion equation is

$$\frac{\partial u}{\partial t} = \frac{1}{\sigma}\left(a - u - \frac{4uv}{1+u^2} + \nabla^2 u\right), \tag{1a}$$

$$\frac{\partial v}{\partial t} = b\left(u - \frac{uv}{1+u^2}\right) + d\nabla^2 v, \tag{1b}$$

where u and v denote the dimensionless concentration of the activator iodide ion (I^-) and inhibitor chlorite (ClO_2^-), respectively; σ, a, and b stand for the control parameters of the reaction kinetics; d is the ratio of diffusion coefficient of inhibitor D_v to that of activator D_u.

The concentration of the iodide ion as well as its diffusion is vital to the CIMA ionic reaction. Assuming that the diffusion coefficients of both substances, D_u and D_v, depend on u, we adopt the diffusivity expression by which both diffusion coefficients relate linearly with the concentration u [34]:

$$D'_u \sim (1 + k_u u), \tag{2a}$$

$$D'_v \sim d(1 + k_v u), \tag{2b}$$

where D'_u and D'_v are the diffusion coefficients of activator u and inhibitor v after introducing a LCDD, respectively; k_u and k_v are the LCDD coefficients in relation to dimensionless concentration u and v, respectively. We set $k_u = k_v = k$ for the sake of simplicity and exclude the influence of the ratio of D'_v to D'_u. Combining Eqs. (2a) and (2b), one can rewrite Eqs. (1a) and (1b) as below:

$$\frac{\partial u}{\partial t} = \frac{1}{\sigma}\left(a - u - \frac{4uv}{1+u^2}\right) + \frac{1}{\sigma}\nabla\cdot[(1+ku)\nabla u], \tag{3a}$$

$$\frac{\partial v}{\partial t} = b\left(u - \frac{uv}{1+u^2}\right) + d\nabla\cdot[(1+ku)\nabla v]. \tag{3b}$$

Equations (3a) and (3b) are employed in this study to explore the influence of a LCDD on the pattern formation of the system by simply adjusting the value of amplitude parameter k.

According to Ref. [36], we set the relative diffusion parameter $\sigma = 50$, $d = 1.07$. The choice of parameters a and b should be in accord with the relative position in the CIMA phase diagram (Fig. 1) [36,37]. In order to realize different types of pattern forms under a LCDD state, we chose three typical points near the critical point region in the phase diagram (Fig. 1): point α ($a = 9.2$, $b = 0.14$) at which both stripe and hexagon spot pattern coexist; point β ($a = 9.5, b = 0.16$) where only stripe pattern occurs; and point γ ($a = 10.5, b = 0.26$) where π-phase hexagon spots dominate over stripes.

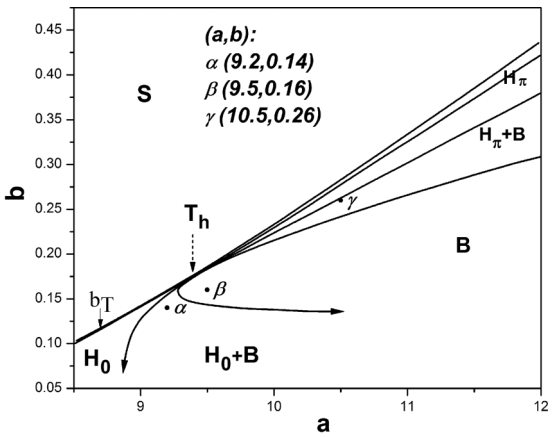

FIG. 1. The schematic phase diagram for pattern selection of the CIMA model (see Rudovics *et al.*, Ref. [36] for details). b_T means the Turing bifurcation line; points α, β, and γ represent three types of different patterns, respectively: $H_0 + B$ (the mixed mode of 0-phase hexagon spot pattern and stripe pattern), B (pure stripe pattern), $H_\pi + B$ (the mixed mode of π-phase hexagon spot pattern and stripe pattern). S denotes a uniform state. T_h represents the bifurcation point of H_0 and H_π, which occurs at $a_h = 9.3908$.

The spatiotemporal equations (3a) and (3b) were solved numerically by using commercial software COMSOL Multiphysics for different evolution times and spatial sizes. A random initialization perturbed around a homogeneous steady state was used as the initial condition and a zero-flux boundary condition was employed. We carry out five independent calculations for each case (unless mentioned particularly) and obtain their statistical average. Generally, all simulations, unless otherwise specified, were performed in 100×100 square grids with a time step of 0.1 arbitrary units. Meanwhile, the relationship between pattern wavelength (λ) and a LCDD coefficient (k) with different system size (L) was also investigated.

B. The method of image processing

A typical method of two-dimensional fast-Fourier transform (2D FFT) was utilized to distinguish the pattern of spots from stripes and acquire the wavelength of pattern. A quantitative image processing method was adopted to quantify the developmental spots in the pattern. By the method of fuzzy C-means clustering (cluster number: 2), both spot and stripe pattern can be separated from the background with a compactness parameter C, which is defined as a spot criterion to discriminate spot from stripe in the pattern:

$$C = \frac{\rho^2}{4\pi S}, \tag{4}$$

where ρ and S represent the perimeter and area of a pending image, respectively [38]. Then we set up a threshold value for classifying the pattern. The pattern is perceived to be the stripe pattern when the compactness of the pending image is larger than the threshold value and vice versa. Finally, after subtracting the background area, we figured out the area of

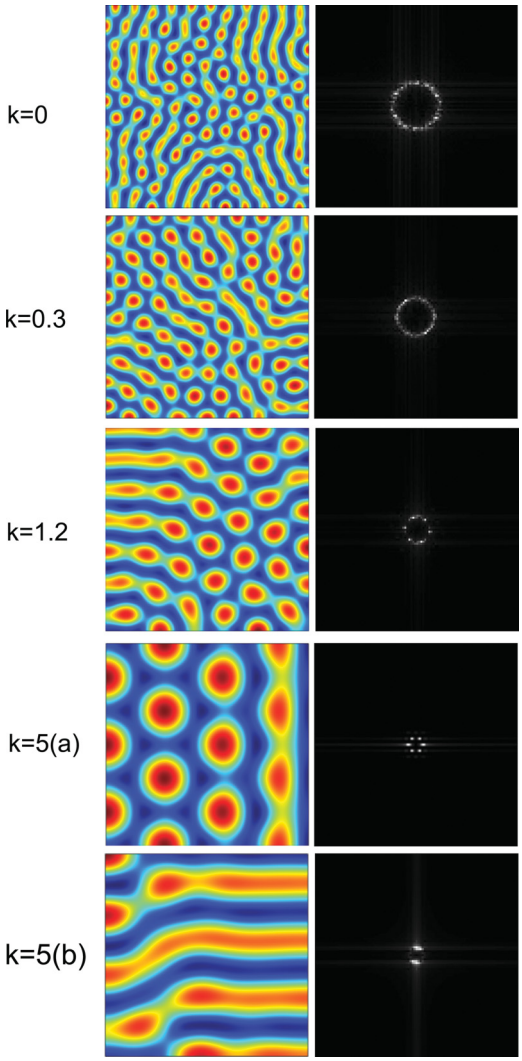

FIG. 2. (Color online) Pattern formation and corresponding 2D fast Fourier transform (FFT) with different concentration-dependent diffusivity k values when the system is located at point α ($a = 9.2$, $b = 0.14$). $k = 5$(a) and $k = 5$(b) stand for the two types of completely different patterns: uniform H_0 spot and stripe patterns, respectively, when $k = 5$ with the same parameter. ($t = 10\,000$ for the first two graphs and $t = 100\,000$ for the last three graphs, system size $L = 100$). Red corresponds to a higher concentration of iodide (u).

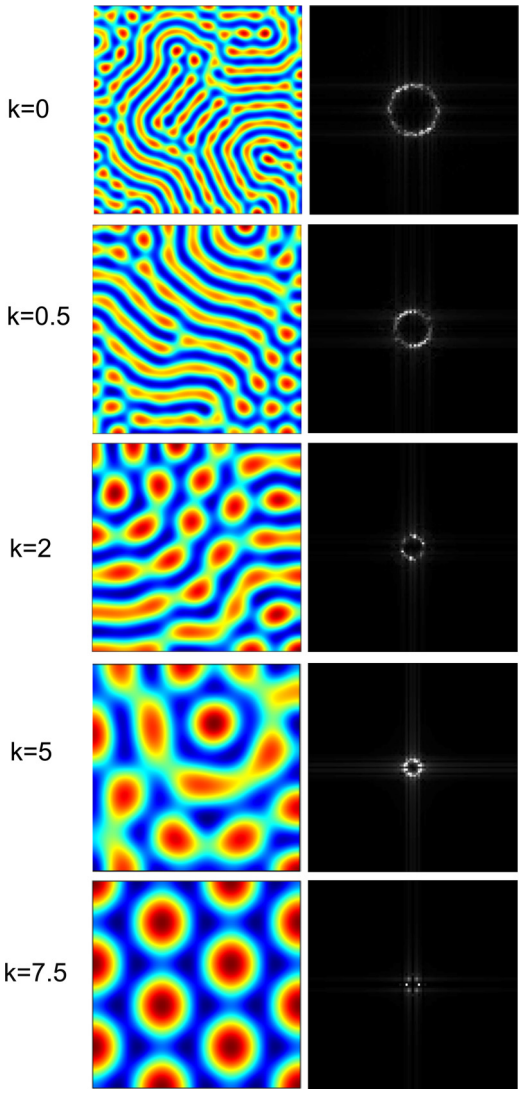

FIG. 3. (Color online) Pattern formation and corresponding 2D fast Fourier transform (FFT) with different concentration-dependent diffusivity k values when the system is located at β ($a = 9.5$, $b = 0.16$) ($t = 10\,000$, except the last graph where $t = 50\,000$, system size $L = 100$). Red corresponds to a higher concentration of iodide (u).

the spot and stripe pattern in the domain and calculated the percentage of them, respectively.

III. RESULTS AND DISCUSSION

A. Regulation of Turing patterns with LCDD

Figures 2– 4 show the snapshots of the evolutional patterns and relevant 2D FFT images when the system is at points α ($a = 9.2, b = 0.14$), β ($a = 9.5, b = 0.16$), and γ ($a = 10.5, b = 0.26$) with various LCDD amplitudes k, respectively. Figures 5(a)–5(c) display the relevant percentage of spot pattern (R) in the snapshots depicted by box plot for the three points above.

At point α: In the absence of a LCDD ($k = 0$), the system pattern takes on a mixed mode (H_0 and B) with a stripe domination (a small R value). On introduction of a LCDD coefficient, namely $k \neq 0$, a remarkable change occurs in the pattern form, i.e., growing spots and thickening stripes, as well as statistically increasing R with k. Note that a broad distribution of R occurs in a large LCDD state. When $k = 5$, the system exhibits a striking difference on the evolution of pattern form in that two distinctive patterns form: a hexagonal spot pattern [$k = 5$(a) in Fig. 2] and a stripe pattern [$k = 5$ (b) in Fig. 2], that evolve from a random initial condition. The 2D FFT images in Fig. 2 demonstrate clearly the transition from a mixed mode with blurred spots to a nearly single mode with either clear hexagonal spots or stripes.

At point β: The spots grow and stripes thicken, and R increases monotonically with k. Nevertheless, the transformation of the system pattern is not as apparent as that of the pattern at point α, and a much larger k is required to realize a clear transition. The 2D FFT images show this transition

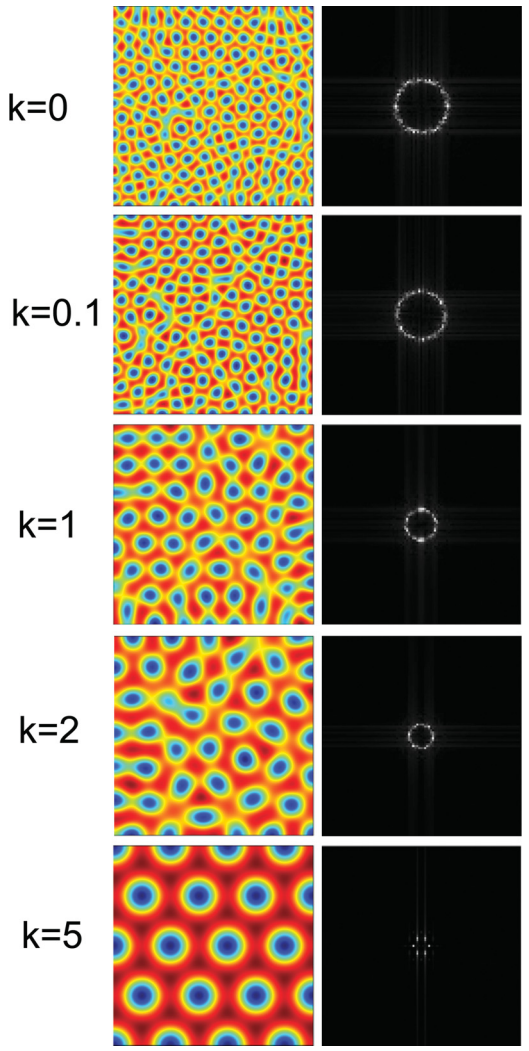

FIG. 4. (Color online) Pattern formation and corresponding 2D fast Fourier transform (FFT) with different concentration-dependent diffusivity k values when the system is located at γ ($a = 10.5$, $b = 0.26$) ($t = 10\,000$ except the last graph where $t = 50\,000$, system size $L = 100$). Blue corresponds to a lower concentration of iodide (u).

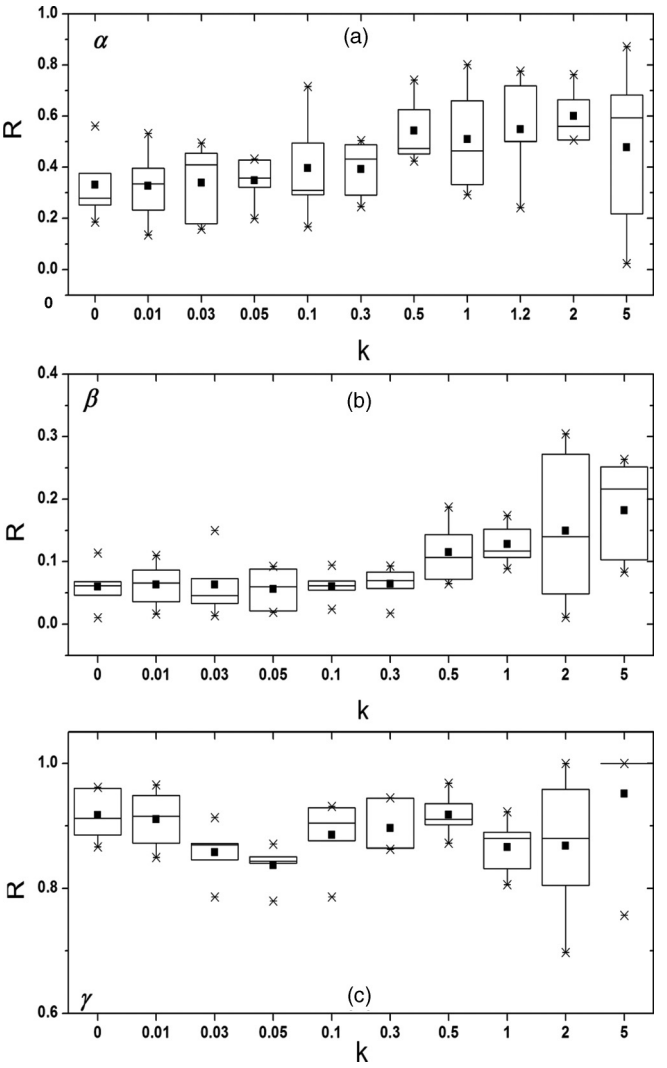

FIG. 5. (a) The box plot of the percentage of spot R with different k values when the system is located at α. In this picture, the box contains the data whose value ranges from rank 25% to rank 75% when we arrange the data in order from small value to large; the solid black square symbol denotes the algebraic mean value of R after five independent calculations; the horizontal line in the box manifests the median of R; the asterisklike symbol stands for extreme values. The median of R increases statistically with k, except at $k = 5$, and the result distribution is scattered broadly. (b) R with different k values when the system is located at β. R increases monotonously with k. All of the results are based on five independent calculations except the case where $k = 2$ or $k = 5$ which experiences ten independent calculations. (c) R with different k values when the system is located at γ. The R fluctuates randomly when k increases from 0 to 2. When $k = 5$, R equals 1, indicating that the system pattern is a uniform array of hexagon spots. All of the result based on five independent calculations except the case where $k = 2$ which experiences ten independent calculations.

clearly. This result shows that the stripe pattern of the pure stripe mode is more robust than that of the mixed mode when the pattern transforms from stripe to spot.

At point γ: The result shows that when $k = 0$, the system pattern is highlighted by a more typical π-phase spot feature. With the increment of k, spots grow but the value of R fluctuates around 0.85. The system evolves steadily into a uniform hexagon spot pattern at $k = 5$. The information in relevant 2D FFT images confirms this transformation precisely.

At point α, owing to the enhancement of the CIMA autocatalyst reaction as well as the involvement of LCDD, the isotropic diffusion of the hexagon pattern occurs more readily than that of the stripe pattern, because the stripe pattern diffuses only in a certain direction under the influence of an enhanced CIMA autocatalyst reaction and LCDD. Consequently, the hexagon spot pattern grows more easily than the stripe pattern with an increasing R when LCDD coefficient k increases in this circumstance. At point β, the situation is similar to that at point α and the system undergoes a transition from stripe to spot also for a larger k. While at point γ, within the range of k from 0 to 2, the system has no remarkable change of pattern form except expanding hexagon spots. It is suggested that the influence of LCDD on the hexagon spot pattern is trivial other than expanding due to its higher stability under LCDD at point

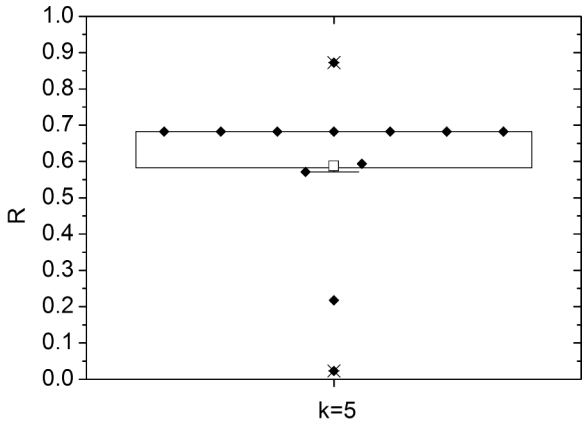

FIG. 6. The box plot with data points of the percentage of spot pattern (R) when $k = 5$, at point α after 12 independent calculations. The horizontal axis label indicates that there is only one case where $k = 5$. The solid diamond and hollow square represent the calculation result and mean value of R, respectively; the asterisklike symbol stands for extreme values. This result indicates that most of data have a larger value of R and the hexagon spot pattern dominates in such system.

γ. This phenomenon is explicable by a greater stability of the hexagonal spot pattern than the stripe pattern under LCDD for pattern transformation at points α and β. Nevertheless, when $k = 5$, the effect of a LCDD is so strong that the system evolves into a larger and uniform hexagonal spot pattern.

Is the explanation above also suitable for the distinctiveness when $k = 5$ at point α (shown in Fig. 2)? It is necessary to collect more data for analyzing this problem from the viewpoint of statistics. Figure 6 shows the broad bistable distribution of R values after repeating 12 independent calculations. Statistically, most of the data points are located above $R = 0.5$, indicating that the two distinctive patterns [shown in Fig. 2, $k = 5$(a) and $k = 5$(b)] do not develop from a random initialization with an equal probability. The hexagon spot [Fig. 2, $k = 5$(a)] pattern dominates the mixed bistable state in the evolution of the LCDD system, namely the preference of a biased bistability. The reason for the preference of a biased bistability at a larger k value is under investigation.

Note that in Fig. 5 the distributions of pattern forms scatter broadly no matter which point (α, β, γ) is concerned. The scattering distribution can be attributed to the use of a non-flux boundary condition [39]. Figure 5 also shows that in the case of a larger k ($k = 2$ or $k = 5$), the resulting distribution also become more scattered. This is because the boundary effect becomes remarkable while pattern wavelength increases and pattern form extends in size at a large value of k. According to Fig. 5, the result distribution at point α is more scattered than that of its counterparts at β and γ; this will be discussed later.

We must emphasize the difference between our pattern regulation and those reported previously [6,14,18] in that our pattern regulation is characterized by a variable pattern wavelength (λ). As for the pattern regulations reported previously, their pattern wavelengths (wave numbers) have no remarkable change regardless of either an intrinsic or extrinsic mode involved. In this study, however, pattern regulation became available with a considerable change of wavelength, which provides a new means to regulate both growth and transformation of spot and stripe pattern while LCDD is included.

Based on the above results and discussion, the pattern regulation of the system with LCDD elicits two fundamental issues for further discussion:

(1) The intrinsic law underlying the pattern regulation and the formula of wave number versus LCDD coefficient k.

(2) The relationship between pattern wavelength (λ) and system size (L).

B. The intrinsic law between pattern wavelength and LCDD coefficient *k*

According to the 2D FFT images from Figs. 2–4, the wave numbers of patterns decrease with increasing LCDD coefficient k, which is similar to the result by Guiu-Souto *et al.* [40]. They studied the manipulation of diffusivity in the Turing system through an external mode and found the decline of wave number with increasing diffusion coefficients. The manipulation of diffusivity in our study is an intrinsic mode and the diffusion coefficients are closely related with the local concentration of reactants. In spite of differences in the mode of manipulating diffusivity, the dependence of the wave number on diffusivity in the Turing system turns out to display a similar trend. Figure 7 shows the pattern wave number ($K = 2\pi/\lambda$, here, uppercase K is used to avoid confusion with the LCDD coefficient k) versus LCDD coefficient k at points α, β, and γ, respectively. Evidently, there is a specific square-root law by which the wave number ($2\pi/\lambda$) is related with LCDD coefficient k near the critical point region:

$$\frac{2\pi}{\lambda} = (c_1 + c_2 k)^{-1/2}, \tag{5}$$

where c_1 and c_2 are curve-fitting constants. To clarify the problem, we performed the linear stability analysis for the traditional CIMA Turing system ($k = 0$) and extended it into the system with LCDD ($k \neq 0$).

Concerning Eqs. (1a) and (1b), the system has a unique uniform steady state, that is, $u_0 = a/5$, $v_0 = 1 + a^2/25$. Now we introduce a pair of perturbations, x and y, to this state:

$$x = u - \frac{a}{5}, \quad y = v - 1 - \frac{a^2}{25}. \tag{6}$$

From Eqs. (1a) and (1b), we can get the linear perturbation:

$$\begin{aligned} \frac{\partial x}{\partial t} &= a_{11}x + a_{12}y + \frac{1}{\sigma}\nabla^2 x, \\ \frac{\partial y}{\partial t} &= a_{21}x + a_{22}y + d\nabla^2 y, \end{aligned} \tag{7}$$

where a_{11}, a_{12}, a_{21}, and a_{22} are the four elements of a Jacobian matrix,

$$J = \begin{pmatrix} a_{11} & a_{12} \\ a_{21} & a_{22} \end{pmatrix} = \begin{pmatrix} \frac{\partial f}{\partial u} & \frac{\partial f}{\partial v} \\ \frac{\partial g}{\partial u} & \frac{\partial g}{\partial v} \end{pmatrix}_{u_0, v_0} = \begin{pmatrix} \frac{-5+\frac{8a^2}{25+a^2}}{\sigma} & \frac{-20a}{(25+a^2)\sigma} \\ \frac{2a^2 b}{25+a^2} & \frac{-5ab}{25+a^2} \end{pmatrix}. \tag{8}$$

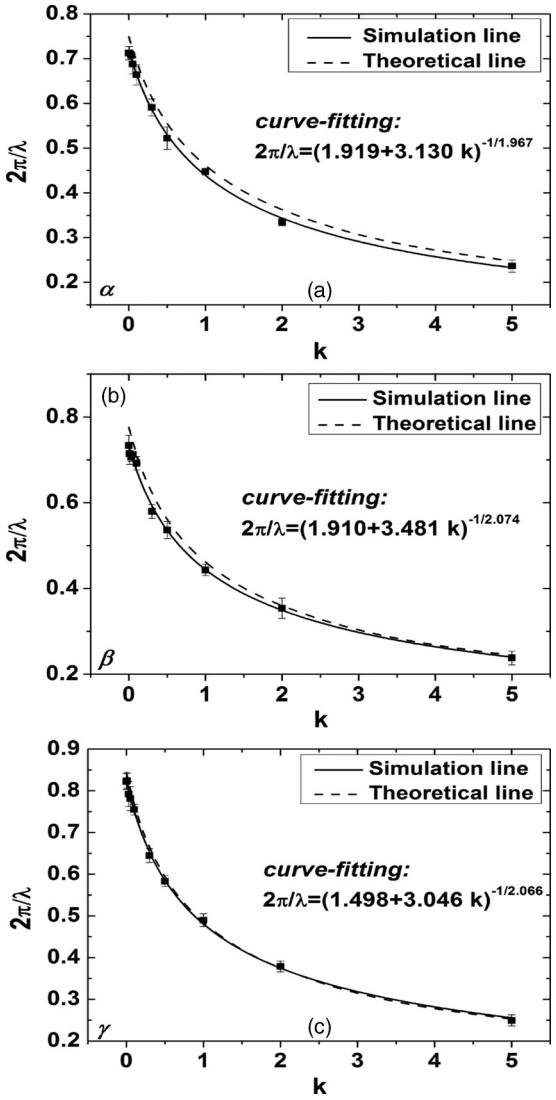

FIG. 7. (a)–(c) The plot of wave number of system pattern versus LCDD coefficient k at points α, β, and γ, respectively. The solid line represents the simulation line (curve-fitting line) while the dashed line denotes the theoretical line derived from Eq. (15).

Then we expand x and y in Fourier space,

$$\begin{pmatrix} x \\ y \end{pmatrix} = \sum_k \begin{pmatrix} c_k^1 \\ c_k^2 \end{pmatrix} e^{\lambda_k t + ikx}, \tag{9}$$

and acquire the characteristic equation:

$$\lambda_k \begin{pmatrix} c_k^1 \\ c_k^2 \end{pmatrix} = \begin{pmatrix} a_{11} - \frac{1}{\sigma}k^2 & a_{12} \\ a_{21} & a_{22} - dk^2 \end{pmatrix} \begin{pmatrix} c_k^1 \\ c_k^2 \end{pmatrix}. \tag{10}$$

The dispersion relation is

$$\lambda_k^2 - \mathrm{tr}_k \lambda_k + \Delta_k = 0, \tag{11}$$

where

$$\mathrm{tr}_k = a_{11} + a_{22} - k^2\left(\frac{1}{\sigma} + d\right),$$

$$\Delta_k = a_{11}a_{22} - a_{12}a_{21} - k^2\left(\frac{1}{\sigma}a_{11} + a_{22}d\right) + \frac{dk^4}{\sigma}. \tag{12}$$

TABLE I. The wave number of pattern from numerical simulations (K) and the critical wave number (K_c) by Eq. (13) when the system is located at points α, β, and γ, respectively.

Point	α	β	γ
K_c	0.7486	0.7756	0.8441
K	0.7124	0.7335	0.8224

The critical wave number is

$$\left(\frac{2\pi}{\lambda_c}\right)^2 = \frac{\sigma d a_{11} + a_{22}}{2d} = K_c^2. \tag{13}$$

Substituting the values of a and b at points α, β, γ into Eq. (13), we can calculate the critical wave number analytically. Since points α, β, γ are located near the Turing bifurcation line, we expect that the wave number of the pattern at points α, β, γ calculated from the numerical simulation ($K = 2\pi/\lambda$, shown in Fig. 7.) is close to the critical wave number ($K_c = 2\pi/\lambda_c$) from Eq. (13). The results are listed in Table I. Consequently, the wave number of the pattern (K) can be treated as the critical wave number (K_c) approximately when $k = 0$.

In the case of $k \neq 0$, the effective diffusion coefficients of u and v are

$$\frac{1}{\sigma} \to \frac{1}{\sigma}(1 + ku), \quad d \to d(1 + ku). \tag{14}$$

After a long time evolution, the development of the system patterns at points α, β, and γ become stationary and the wave numbers stay fixed at a certain k regardless of either a zero or nonzero k value, as shown in Fig. 8. This is important evidence that the pattern form of the system with LCDD still retains the basic nature of the classic Turing pattern; therefore the system with LCDD could be regarded as an equivalent Turing system. According to the properties of the system pattern, the pattern wavelength is a constant that does not change with local concentration u. As a result, the LCDD effect on pattern wave number should be "constantized" and we need to define a constant u_e (equivalent local concentration induced by LCDD)

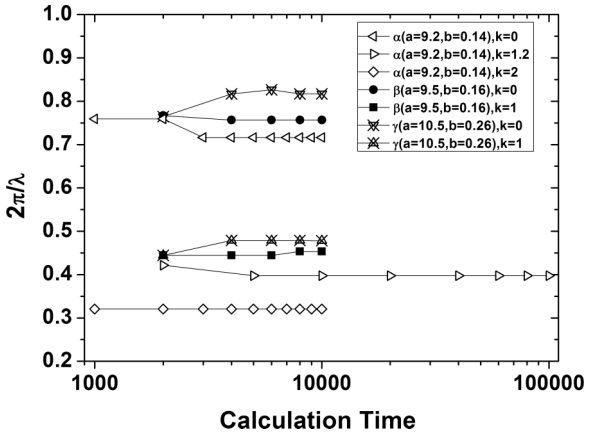

FIG. 8. The wave number of simulated pattern versus evolution time with different k values when system is located at points α, β, and γ, respectively.

TABLE II. The equivalent local concentration of pattern (u_e), uniform steady state (u_0), and their relative deviation (E) at points α, β, and γ, respectively.

Point	α	β	γ
u_0	1.840	1.900	2.100
u_e	1.631	1.823	2.033
E	11.36%	4.05%	3.19%

to characterize and average the LCDD effect on pattern wave number with different u. The pattern wave number of the system with LCDD is expressed as below:

$$\frac{2\pi}{\lambda} = K = \sqrt{\frac{\sigma d a_{11} + a_{22}}{2d(1+ku_e)}} = K_c\sqrt{\frac{1}{1+ku_e}} \propto (1+ku_e)^{-1/2}, \tag{15}$$

by which the square-root law [Eq. (5)] can be derived successfully. Comparing Eq. (15) with Eq. (5), we can work out $u_e = c_2/c_1$ at points α, β, and γ, respectively. A new parameter E was defined to characterize the relative deviation of u_e from the uniform steady state u_0 :

$$E = \frac{|u_e - u_0|}{u_0}. \tag{16}$$

The calculated results are listed in Table II. Here, $a = 9.2$, 9.5, and 10.5 were used for the calculation of u_0 at points α, β, and γ, respectively; $c_{1\alpha} = 1.919$, $c_{2\alpha} = 3.130$, $c_{1\beta} = 1.910$, $c_{2\beta} = 3.481$, $c_{1\gamma} = 1.498$, and $c_{2\gamma} = 3.046$ from Fig. 7 were employed to calculate the u_e approximately at points α, β, and γ, respectively.

Note that E_α is larger than E_β and E_γ, which is consistent with the broadest distribution of R at point α after introducing a LCDD. Considering generally, the combination of the three factors listed below, in addition to bistability, are also probably responsible for the extreme scattering of the pattern form at point α when $k = 5$ (Figs. 2 and 5):

(1) Non-flux boundary condition;

(2) Strong boundary effect induced by drastic change of pattern wavelength (λ) when $k = 5$;

(3) The largest divergence between u_e and u_0.

The parameter u_e is introduced as a substitution variable to characterize the LCDD Turing system, and it provides a feasible way to study the LCDD Turing system analytically.

The results of both Fig. 8 and Eq. (15) suggest that the pattern formation of the system with LCDD still holds the character of Turing patterns when $L = 100$, which differs from the result of Roussel and Wang [35,36]. Their work shows that a new type of pattern different from the traditional Turing pattern emerges after introducing the LCDD in excitable medium based on the Gray-Scott model.

We explore the pattern wavelength λ and system size L under conditions of various k values in order to reveal the combinational effect of both L and k on pattern development. The system wavelengths λ increase with k but are independent of system size except at small L as displayed in the inset of Fig. 9. This is consistent with the feature of stationary Turing pattern shown in Fig. 8. Furthermore, we rescaled λ against k

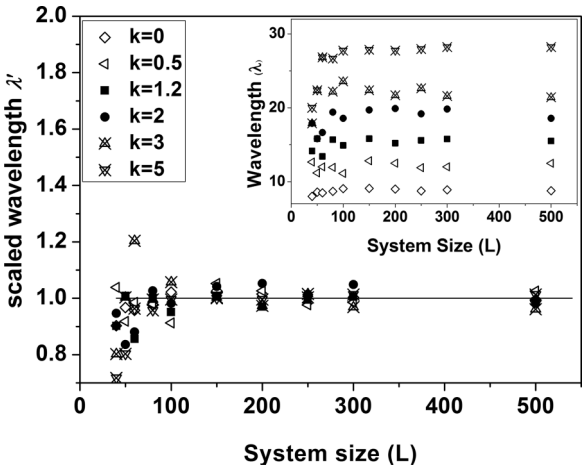

FIG. 9. The scaled wavelength (λ') versus L by square-root law. (Inset) The plot of pattern wavelength (λ) and system size (L) with different k values when system is located at point α ($a = 9.2$, $b = 0.14$).

using the intrinsic square-root law between λ and k [Eq. (5), Fig. 7] and acquired the scaled wavelength λ':

$$\lambda' = \frac{\lambda}{(78.54074 + 139.41879k)^{1/2}}. \tag{17}$$

Figure 9 shows that scaled wavelengths λ' versus L for different k clearly approach the line $\lambda' = 1$ when $L \geqslant 80$. The rescaling λ against k, namely elimination of the LCDD coefficient, not only manifests the size dependence of the wavelength of the Turing system with LCDD, but also verifies the fundamentality of intrinsic square-root law between λ and k in the Turing system with LCDD. And it also proves the self-consistency of the analysis above.

Overall, our study confirms that for the Turing system which involves a local concentration-dependent diffusivity, it is possible for the system pattern to maintain the characteristics of the traditional Turing pattern in a wide range of LCDD coefficient k.

IV. CONCLUSIONS

We study the evolution and regulation of the pattern form in the CIMA Turing system modified by a local concentration-dependent diffusivity (LCDD), which is referred to as an equivalent Turing system and has a fundamental significance for physical, chemical, and biological systems with heterogeneity. The evolutional patterns of the system are regulated by adjusting the LCDD coefficient k systematically and are quantitatively evaluated through the image processing procedure of fuzzy C-means clustering. The introduction of LCDD in a Turing system serves as an important intrinsic means for pattern regulation through altering pattern wavelength, and it can bring about the pattern transformation from stripe to hexagon spot at point α (in the pattern area of $H_0 + B$), β (in the pattern area of B), and γ (in the pattern area of $H_\pi + B$). There is an intrinsic square-root law relating to the pattern wavelength (λ) and LCDD coefficient k, and we extend

the linear stability analysis into the system with LCDD to explain such law. The system wavelength is invariant with the system size ($L \geqslant 80$) and can be well rescaled by the LCDD coefficient k. The method that we employ for pattern regulation, in itself, has certain biophysical significance in that it suggests a potential mechanism for modeling the expanding spots and stripes in the biological matrix with constant size. These results are beneficial to interpreting the development of some biological patterns with special size and shape, and exploring the intrinsic laws in a complicated biological matrix.

ACKNOWLEDGMENTS

All authors of this paper would like to express their gratitude to Dr. Bao-Quan Ai for his valuable comments and English revision to this paper. This work is supported by the National Natural Science Foundation of China (Grant No. 10875178), the Fundamental Research Funds for the Central Universities, and Specialized Research Fund for the Doctoral Program of Higher Education (Grant No. 20110171110023). Z.W.R. would also like to thank the support of the Fundamental Research Funds for the Central Universities, JNU (Grant No. 21611437).

[1] A. M. Turing, Philos. Trans. R. Soc., B **237**, 37 (1952).
[2] V. Castets, E. Dulos, J. Boissonade, and P. De Kepper, Phys. Rev. Lett. **64**, 2953 (1990).
[3] I. Lengyel and I. R. Epstein, Science **251**, 650 (1991).
[4] R. A. Barrio, C. Varea, J. L. Aragón, and P. K. Maini, Bull. Math. Biol. **61**, 483 (1999).
[5] R. T. Liu, S. S. Liaw, and P. K. Maini, Phys. Rev. E **74**, 011914 (2006).
[6] R. A. Barrio, R. E. Baker, B. Vaughan, K. Tribuzy, M. R. de Carvalho, R. Bassanezi, and P. K. Maini, Phys. Rev. E **79**, 031908 (2009).
[7] S. Kondo and R. Asai, Nature **376**, 765 (1995).
[8] S. Miyazawa, M. Okamoto, and S. Kondo, Nature Commun. **1**, 1 (2010).
[9] A. P. Muñuzuri, M. Dolnik, A. M. Zhabotinsky, and I. R. Epstein, J. Am. Chem. Soc. **121**, 8065 (1999).
[10] M. Dolnik, A. M. Zhabotinsky, and I. R. Epstein, Phys. Rev. E **63**, 026101 (2001).
[11] D. G. Míguez, S. Alonso, A. P. Muñuzuri, and F. Sagués, Phys. Rev. Lett. **97**, 178301 (2006).
[12] B. Schmidt, P. De Kepper, and S. C. Müller, Phys. Rev. Lett. **90**, 118302 (2003).
[13] S. S. Riaz, S. Kar, and D. S. Ray, J. Chem. Phys. **121**, 5395 (2004).
[14] W. Q. Chen, H. Zhang, H. P. Ying, B. W. Li, and J. X. Chen, J. Chem. Phys. **127**, 154708 (2007).
[15] F. Lesmes, D. Hochberg, F. Morán, and J. Pérez-Mercader, Phys. Rev. Lett. **91**, 238301 (2003).
[16] H. Wang, K. Zhang, and Q. Ouyang, Phys. Rev. E **74**, 036210 (2006).
[17] H. Wang, Z. Fu, X. Xu, and Q. Ouyang, J. Phys. Chem. A **111**, 1265 (2007).
[18] S. Alonso and F. Sagués, Phys. Rev. E **80**, 035203(R) (2009).
[19] J. D. Murray, *Mathematical Biology* (Springer-Verlag, Berlin, 1989).
[20] C. J. Roussel and M. R. Roussel, Prog. Biophys. Mol. Biol. **86**, 113 (2004).
[21] S. B. Yuste, E. Abad, and K. Lindenberg, Phys. Rev. E **82**, 061123 (2010).
[22] A. Eldar, D. Rosin, B.-Z. Shilo, and N. Barkai, Dev. Cell **5**, 635 (2003).
[23] P. V. Gordon, C. Sample, A. M. Berezhkovskii, C. B. Muratov, and S. Y. Shvartsman, Proc. Natl. Acad. Sci. USA **108**, 6157 (2011).
[24] H. Shoji, Y. Iwasa, A. Mochizuki, and S. Kondo, J. Theor. Biol. **214**, 549 (2002).
[25] H. Shoji, A. Mochizuki, Y. Iwasa, M. Hirata, T. Watanabe, S. Hioki, and S. Kondo, Dev. Dyn. **226**, 627 (2003).
[26] H. Shoji, Y. Iwasa, and S. Kondo, J. Theor. Biol. **224**, 339 (2003).
[27] S. Ishihara and K. Kaneko, J. Theor. Biol. **238**, 683 (2006).
[28] H. Shoji and Y. Iwasa, J. Theor. Biol. **237**, 104 (2005).
[29] Y. Osada and A. R. Khokhlov, *Polymer Gels And Networks* (Marcel Dekker, Inc. New York–Basel, 2002), p.167.
[30] C. Wagner, Trans AIME, J. Metals **4**, 91 (1952).
[31] A. Okubo, *Diffusion and Ecological Problems: Mathematical Models* (Springer-Verlag, Berlin, 1979).
[32] A. L. Horwath, *Handbook of Aqueous Electrolyte Solutions* (Ellis Horwood, Chichester, UK, 1986), p. 285.
[33] H. Malchow, J. Theor. Biol. **135**, 371 (1988).
[34] M. R. Roussel and J. Wang, Phys. Rev. Lett. **87**, 188302 (2001).
[35] M. R. Roussel and J. Wang, J. Chem. Phys. **120**, 8079 (2004).
[36] Q. Li, C. Zheng, N. Wang, and B. Shi, J. Sci. Comput. **16**, 121 (2001).
[37] B. Rudovics, E. Barillot, P. W. Davies, E. Dulos, J. Boissonade, and P. De Kepper, J. Phys. Chem. A **103**, 1790 (1999).
[38] R. C. Gonzalez and R. E. Woods, *Digital Image Processing*, 2nd ed. (Prentice Hall, New Jersey, 2002).
[39] P. Arcuri and J. D. Murray, J. Math. Biol. **24**, 141 (1986).
[40] J. Guiu-Souto, J. Carballido-Landeira, V. Pérez-Villar, and A. P. Muñuzuri, Phys. Rev. E **82**, 066209 (2010).